IEEE Access
Multidisciplinary | Rapid Review | Open Access Journal

Date of publication xxxx 00, 0000, date of current version xxxx 00, 0000.

Digital Object Identifier 10.1109/ACCESS.2017.Doi Number

Dynamic ADC Resolution-Mapping for Millimeter-Wave Massive MIMO Systems

Chia-Chang Hu[1], Member, IEEE, Yong-Siang Li[2], and Chen-Yueh Lin[3]

[1]National Department of Communications Engineering, National Chung Cheng University, Chia-Yi, Taiwan
[2] National Department of Communications Engineering, National Chung Cheng University, Chia-Yi, Taiwan
[3] National Department of Communications Engineering, National Chung Cheng University, Chia-Yi, Taiwan

e-mail:jameshu183@gmail.com

This paragraph of the first footnote will contain support information, including sponsor and financial support acknowledgment. For example, “This work was supported in part by the U.S. Department of Commerce under Grant BS123456.”

ABSTRACT The radio-frequency (RF) chains, phase shifters (PSs), and analog-to-digital converters (ADCs) play the dominant role of power consumption in the uplink hybrid millimeter-wave (mmWave) massive multiple-input multiple-output (MIMO) networks. To mitigate power consumption, an energy-efficient switch and inverter (SI) based partially-connected (PC) architecture with the Gram-Schmidt (GS) antenna selection strategy is addressed. The design of a variable-resolution ADC configuration is addressed under an independent upper bound of power consumption for each ADC in this paper. However, the resulting ADC resolution mapping becomes more complicated due to variant ADC power bounds. A simple ADC bit-allocation algorithm, namely, the sum-resolution (SR) ADC, is proposed.By replacing the total power constraint on ADCs to improve both the achievable sum-rate (ASR) and energy efficiency (EE) performance of the hybrid mmWave massive MIMO system. The SR-ADC solutions in closed form reveal that the optimal ADC resolution is proportional to the square power of the signal-to-noise ratio (SNR) in RF chains. Simulation results demonstrate that the proposed SR-ADC approach offers enhanced improvements on the ASR and EE, and exhibits prominent advantages on the number of activated RF chains compared with the fixed total power system.

INDEX TERMS ADC, energy efficiency, massive MIMO, mmWave, partially-connected architecture

I. INTRODUCTION

Owing to the saturation of consumer wireless systems on most sub-6 GHz spectrum, millimeter-wave (mmWave) communication (30-300GHz) has become a key solution to fulfill high data rates in the fifth-generation (5G) broadband networks [1]. The smaller mmWave frequency wavelengths allow of facilitating a large-scale antenna array (LSAA) at the base station (BS) to conquer propagation path-loss and enhance beamforming gain [2]. The massive multiple-input multiple-output (MIMO) configuration constructed by an LSAA amplifies amounts of phase shifters (PSs), analog-to-digital converters (ADCs), and dedicated radio-frequency (RF) chains, which bring about a heavy burden on hardware implementation and energy dissipation [3]. Consequently, to lessen hardware complexity and power consumption more effectively converts into a principal subject for accomplishing the practical mmWave massive MIMO system.

A. RELATED WORKS AND MOTIVATIONS

To mitigate the all-inclusive power consumption in massive MIMO hybrid precoding/combining mmWave systems can be categorized into three classifications. In the first classification, existing literatures concentrate on lowering the power consumption incurred by the PS network (PSN) [2]-[4]. In [2], a finite-resolution PSN is being substituted for the high-precision PSN to alleviate energy consumption fractionally. However, the hardware load remains intense. The less power-consuming network of switches exploited in [3] is utilized to take the place of the PSN. Simulation results demonstrate that the power consumption is lower effectively but the performance degradation of achievable sum-rate (ASR) is incurred. As a result, the switch and inverter (SI) based network is employed in [4] to enhance the energy efficiency (EE) performance at the cost of a slight ASR performance degradation.

In the second group, the target aims at relaxing impacts on the power-demanding ADC since the power expenditure grows exponentially with the number of its quantization

bits. The hybrid mmWave massive MIMO systems with the use of low-precision ADCs have attracted great attention due to capabilities on decreasing hardware complexity and power consumption [5]-[11]. The low-resolution digital-to-analog converter (DAC) structures with fully/partially connected PSNs are investigated in a single-user (SU) mmWave massive MIMO system [5]. In [6], a fully-connected (FC) mapping structure of hybrid precoding with low-resolution ADCs/DACs is explored for the mmWave large-scale MIMO system. The uplink spectral efficiency (SE) of single-cell multi-user (MU) massive MIMO systems with low-resolution ADCs is studied by using the zero-forcing (ZF) detectors over Rician fading channels in [7]. Based on the minimum mean square error (MMSE) approach, the transmitter optimization is addressed for MIMO channels with full channel state information (CSI) when operating under the presence of DAC nonlinearity [8]. The lower bound on the mutual information in MIMO channels with coarse quantization and correlated noise is studied by employing the Bussgang decomposition [9]. However, it is noticed that the use of low-resolution ADCs results in performance degradation in the high signal-to-noise ratio (SNR) regime. As a result, a mixture of low and high precision ADCs is conducted in [10]-[12] to approach a more appropriate trade-off between the ASR and EE. To achieve the optimized EE forthright, both the exhaustive algorithm (EA) and the greedy algorithm (GA) are proposed in [13] on a basis of the EE maximization criterion. The flexible ADC bit-allocation (BA) mechanism with optional constraint bits, namely MMSQE-BA [14], is proposed and produces superior performance than that of a fixed-ADC configuration. With the objective of maximizing EE at the BS, the design of resolution-adaptive ADC bit-allocation is presented for uplink multiuser large-scale MIMO systems in [15]. A hybrid beamforming architecture consisting of less number of RF chains with the coordinate update algorithm (CUA) based variable-resolution ADCs [16] is explored for mmWave massive multiuser MIMO uplink systems. In [17], to jointly optimize the beamspace hybrid combiner and the ADC quantization bit-allocation in order to maximize the system EE is proposed for the uplink multi-user massive MIMO mmWave system.

In the third category, the target focuses on reducing the number of hardware components to achieve lower power consumption. The contiguous subarray correlation (CSC) algorithm proposed in [18] is designed to improve EE performance by migrating the border of the subarray based on the correlation of antenna subarrays. In [19]-[20], the antenna selection (AS) technologies based on the Gram-Schmidt orthogonalization (GSO) process is proposed, which reduces the quantity of PSs by decreasing the activated antennas at the expense of a little system capacity loss.

It is seen from the existing literatures [10]-[12] that a mixed-mode ADC network offers better performance on the ASR and EE than those of the architectural completely-inflexible ADCs. Although the EA and GA achieve the optimal EE performance, the high computation complexity, which scales exponentially with the number of RF chains, is unaffordable for the mmWave systems. In the MMSQE-BA, the quantization bits derived from the closed form solution are adopted to minimize the mean square quantization error (MSQE) under a total ADC power constraint, from which equivalent quantization bits are distributed into RF chains. Motivated by this fixed-resolution ADC architecture, two new ADC bit-allocation schemes named sum-resolution ADC (SR-ADC) and CVX based are developed. This SR-ADC approach determines its quantization bit-distribution according to the average constraint bit and channel gains. The fixed power-bound constraint on the ADC resolution is replaced with a total ADC number. Compared to the MMSQE-BA, the SR-ADC is able to provide a closed form solution with low computation complexity and sustain the flexibility on ADC bit-mapping. The CVX-based algorithm considers the appearance of the extreme resolution allocation, which is overly concentrated on one of ADCs due to the extreme channel condition. Therefore, it is reasonable to make restrictions on the quantization bits for each pair of ADCs. However, the revised optimization problem exists no closed form solution owing to the multiple simultaneous constraints. Fortunately, it can be solved by applying the CVX toolbox.

B. CONTRIBUTIONS

In this paper, two new ADC resolution allocation schemes are investigated for mmWave massive MIMO systems. The results and main contributions of this paper are summarized as follows:

1) Instead of a pre-defined upper bound of ADC power consumption in [14], a total ADC resolution number is used to be a constraint in this paper. The difference between the two assumptions is whether each ADC exists the constraint bits upper bound, wherein ADC power consumption is concerned with the square power of constraint bits. Owing to the difficulty of designing the ADC bit-mapping configuration under an independent power upper bound, the independent constraint bit is replaced by a total amount on ADC resolution, which has no assumption of power upper bound for each ADC.
2) To improve the MMSQE-BA proposed in [14], two new ADC bit-allocation schemes named the CVX based and the SR-ADC are developed. Both of algorithms yield the better ASR and EE performance than the MMSQE-BA for the architectures with the same amount of hardware costs and a slightly increase in computational complexity. In addition, the SR-ADC possesses the lower computation complexity while compared to the CVX method. The existence of the exponential and logarithmic functions in an optimization problem introduces the cumbersome solving processes in the CVX toolbox. As a

consequence, the SR-ADC is more appealing than the CVX. Moreover, simulation results show that the SR-ADC and CVX approaches provide better ASR and EE performance than that of the MMSQE-BA under various numbers of RF chains. With the employment of different architectures, it is demonstrated that the SR-ADC offers the superior EE performance than the CVX when the PSN is used. In the SI-based system, the EE performance gap between the SR-ADC and CVX is unobvious.

3) It is worth noting that the system integration of dynamically-mapped ADC bit resolution and dynamically-connected subarray configuration is developed for the mmWave massive MIMO system in this paper. Owing to such an exclusive combination architecture, the hybrid-mode precoder/combiner system possesses an excellent advantage of reducing the hardware cost significantly at the expense of only slight ASR performance degradation. Compared with the pre-determined sub-connected configuration, the proposed adaptive subarray structure achieves ASR performance approaching the fully-connected pattern. Additionally, the proposed system structure takes the GS antenna selection strategy into consideration for the networks of the SI and PS based analog RF combiner architectures. With the installation of the GS AS strategy, the complexity of the RF chain-antenna mapping operation decreases substantially due to the reduction of the rank of the mmWave MIMO channel matrix. Simulation results demonstrate that an adaptive subarray arrangement in conjunction with the GS-based AS strategy is able to accomplish the EE performance much better than those of approaches without the GS AS with an alleviated demand on both computation and hardware complexities.

Notations: $\mathbf{A}$, $\mathbf{a}$, and a represent a matrix, a vector, and a scalar, respectively. The superscripts $\mathbf{A}^{\mathrm{T}}$, $\mathbf{A}^{\mathrm{H}}$, and $\mathbf{A}^{-1}$ define, respectively, transpose, Hermitian transpose, and inversion operations of a matrix $\mathbf{A}$. $\|\mathbf{A}\|_{\mathrm{F}}$ is the Frobenius norm of $\mathbf{A}$. $\mathbb{R}$, $\mathbb{C}$, and $\mathbb{Z}$ indicate the sets of real numbers, complex numbers, and integers, respectively. $\mathbf{I}_m$ is the identity matrix of size $m \times m$. $\langle \mathbf{a}, \mathbf{b} \rangle$ stands for the inner product of vectors $\mathbf{a}$ and $\mathbf{b}$. E[A] denotes the expected value of A. $\mathcal{CN}(0,\sigma^2)$ means a complex Gaussian distribution with zero mean and variance σ^2.

II. SYSTEM MODEL AND QUANTIZATION MODEL

A. SYSTEM MODEL

Consider a single-user mmWave massive MIMO system based on the clustered Saleh-Valenzuela (SV) channel model with N_{S} data streams as depicted in Fig.1. The transmitter and receiver are, respectively, equipped with N_{T} antennas, $N_{\mathrm{RF}}^{\mathrm{T}}$ RF chains, N_{R} antennas, and $N_{\mathrm{RF}}^{\mathrm{R}}$ RF chains. It is assumed that the conditions of $N_{\mathrm{T}} \geq N_{\mathrm{R}}$, $N_{\mathrm{T}} \geq N_{\mathrm{RF}}^{\mathrm{T}} \geq N_{\mathrm{S}}$, and $N_{\mathrm{R}} \geq N_{\mathrm{RF}}^{\mathrm{R}} \geq N_{\mathrm{S}}$ are satisfied. The functional networks of the SI and PS based analog RF combiner architectures in Fig. 1 are described in Fig. 2(a) and (b), respectively. The SV narrowband mmWave MIMO channel matrix $\mathbf{H}$ of size $N_{\mathrm{R}} \times N_{\mathrm{T}}$ with P rays and I clusters is described as follows:

$$\mathbf{H} = \beta \sum_{i=1}^{I} \sum_{p=1}^{P} \alpha_{ip} \boldsymbol{\Gamma}_{\mathrm{R}}\left(\phi_{\mathrm{R}}^{ip}, \theta_{\mathrm{R}}^{ip}\right) \boldsymbol{\Gamma}_{\mathrm{T}}^{\mathrm{H}}\left(\phi_{\mathrm{T}}^{ip}, \theta_{\mathrm{T}}^{ip}\right), \tag{1}$$

where $\beta = \sqrt{N_{\mathrm{T}} N_{\mathrm{R}} / PI}$ is a normalization factor. Additionally, $\alpha_{ip} \sim \mathcal{CN}(0,1)$, ϕ_{R}^{ip} $(\theta_{\mathrm{R}}^{ip})$, and ϕ_{T}^{ip} $(\theta_{\mathrm{T}}^{ip})$ stand for the complex gain, the azimuth (elevation) angles of arrival and departure (AoAs and AoDs) of the p-th ray in the i-th cluster, respectively. $\boldsymbol{\Gamma}_{\mathrm{R}}\left(\phi_{\mathrm{R}}^{ip}, \theta_{\mathrm{R}}^{ip}\right)$ and $\boldsymbol{\Gamma}_{\mathrm{T}}\left(\phi_{\mathrm{T}}^{ip}, \theta_{\mathrm{T}}^{ip}\right)$ represent the normalized array response vectors at the transmitter and receiver, respectively. The array response vectors of a uniform square planar array (USPA) with $\sqrt{N} \times \sqrt{N}$ antenna array size associated with the p-th ray in the i-th cluster can be written as

$$\boldsymbol{\Gamma}_{\mathrm{USPA}}(\phi^{ip}, \theta^{ip}) = \frac{1}{\sqrt{N}} \Big[1, \ldots, e^{jwd\left(u \sin\phi^{ip} \sin\theta^{ip} + v \cos\theta^{ip}\right)}, \ldots, e^{jwd\left(\left(\sqrt{N}-1\right)\sin\phi^{ip} \sin\theta^{ip} + \left(\sqrt{N}-1\right)\cos\theta^{ip}\right)}\Big]^{\mathrm{T}}, \tag{2}$$

where $0 \leq u < \sqrt{N}$ and $0 \leq v < \sqrt{N}$ are the antenna indices in the two-dimensional planar array. Here, λ, d, $w \triangleq 2\pi/\lambda$, and N denote, respectively, the wavelength, antenna spacing, wave number, and antenna number at the transmitter and receiver ($N = N_{\mathrm{T}}$ or N_{R}).

B. SIGNAL AND QUANTIZATION MODEL

The N_{S}-dimensional data stream $\mathbf{s} \in \mathbb{C}^{N_{\mathrm{S}} \times 1}$ is forwarded by the transmitter. $\mathbf{F}_{\mathrm{D}} \in \mathbb{C}^{N_{\mathrm{RF}}^{\mathrm{T}} \times N_{\mathrm{S}}}$ expresses the digital baseband precoder, and $\mathbf{F}_{\mathrm{A}} \in \mathbb{C}^{N_{\mathrm{T}} \times N_{\mathrm{RF}}^{\mathrm{T}}}$ denotes an RF analog precoder. After joint RF/baseband precoding, the transmit signalvector $\mathbf{x} \in \mathbb{C}^{N_{\mathrm{T}} \times 1}$ is expressed as

$$\mathbf{x} = \mathbf{F}_{\mathrm{A}} \mathbf{F}_{\mathrm{D}} \mathbf{s}, \tag{3}$$

where the transmitted symbol vector $\mathbf{s} \sim \mathcal{CN}\left(0, \mathbf{I}_{N_{\mathrm{S}}}\right)$ is Gaussian distributed with zero mean and unit variance. The hybrid precoders are assumed to meet the power constraint of $\| \mathbf{F}_{\mathrm{A}} \mathbf{F}_{\mathrm{D}} \|_{\mathrm{F}}^2 \leq P_{\mathrm{T}}$, where P_{T} is the total transmit power. At the receiver, the signal vector at the output of the RF combiner $\mathbf{W}_{\mathrm{A}} \in \mathbb{C}^{N_{\mathrm{R}} \times N_{\mathrm{RF}}^{\mathrm{R}}}$ becomes

This article has been accepted for publication in a future issue of this journal, but has not been fully edited. Content may change prior to final publication. Citation information: DOI 10.1109/ACCESS.2021.3070116, IEEE Access

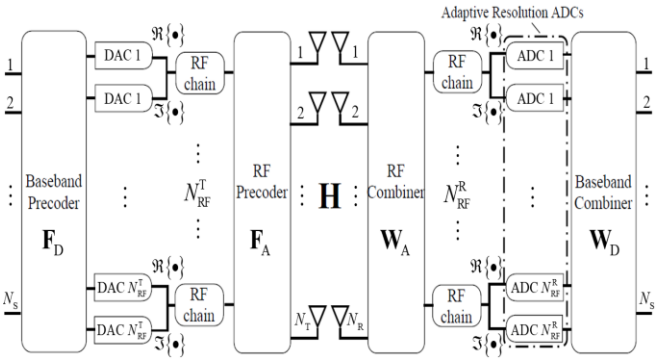

FIGURE 1. MmWave massive MIMO systems with mixed-precision ADCs.

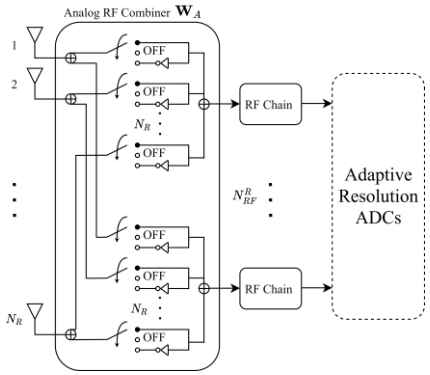

(a)

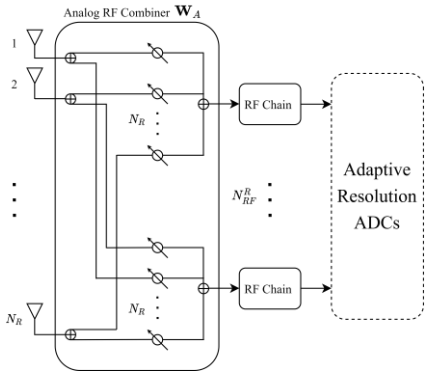

(b)

FIGURE 2. (a) SI, (b) PS based analog RF combiner structures.

$$\mathbf{y} = \mathbf{W}_{\mathrm{A}}^{\mathrm{H}}\mathbf{H}\mathbf{x} + \mathbf{W}_{\mathrm{A}}^{\mathrm{H}}\mathbf{n}, \tag{4}$$

where $\mathbf{n} \sim \mathcal{CN}\left(0, \sigma_{\mathrm{n}}^2 \mathbf{I}_{N_{\mathrm{R}}}\right) \in \mathbb{C}^{N_{\mathrm{R}} \times 1}$ denotes a zero-mean circularly symmetric complex Gaussian (ZMCSCG) noise vector whose entries follow the independent identically distribution (i.i.d.) and the noise power is σ_{n}^2. By applying the additive quantization noise (AQN) model [9], the signal vector received at the output of the baseband combiner $\mathbf{W}_{\mathrm{D}} \in \mathbb{C}^{N_{\mathrm{RF}}^{\mathrm{R}} \times N_{\mathrm{S}}}$ is written as

$$\mathbf{y}_{\mathrm{AQN}} = \mathbf{W}_{\mathrm{D}}^{\mathrm{H}} \mathcal{Q}(\mathbf{y}) \tag{5a}$$

$$= \mathbf{W}_{\mathrm{D}}^{\mathrm{H}} \mathbf{A}_{\alpha} \mathbf{y} + \mathbf{W}_{\mathrm{D}}^{\mathrm{H}} \mathbf{e} \tag{5b}$$

$$= \bar{\mathbf{H}}\mathbf{x} + \bar{\mathbf{n}}, \tag{5c}$$

where $\mathcal{Q}(\cdot)$ defines an element-wise quantization operator, $\mathbf{A}_{\alpha}$ is a diagonal matrix with the diagonal entries $1-\rho_{b_m}$. Here, ρ_{b_m} expresses the quantization distortion factor corresponding to the input-output of the *m*-th quantizer, which is defined as $\rho_{b_m} = \mathrm{E}[(Q(y_m) - y_m)^2] / \mathrm{E}[|y_m|^2]$. Table I provides values of ρ_{b_m} for different quantization bits *b* [21]. The quantization noise vector $\mathbf{e} \in \mathbb{C}^{N_{\mathrm{RF}}^{\mathrm{R}} \times 1}$ obeys the Gaussian distribution and satisfies $\mathrm{E}[\mathbf{y}\mathbf{e}^{\mathrm{H}}]=\mathrm{E}[\mathbf{e}\mathbf{y}^{\mathrm{H}}]=\mathbf{0}$. The covariance matrix is $\mathbf{R}_{\mathrm{e}} = \mathbf{A}_{\alpha}\mathbf{B}_{\alpha}\mathrm{diag}(\mathbf{W}_{\mathrm{A}}^{\mathrm{H}}\mathbf{H}\mathbf{R}_{\mathrm{xx}}\mathbf{H}^{\mathrm{H}}\mathbf{W}_{\mathrm{A}} + \sigma_{\mathrm{n}}^2\mathbf{W}_{\mathrm{A}}^{\mathrm{H}}\mathbf{W}_{\mathrm{A}})$ [22]. Note that $\mathbf{B}_{\alpha}$ forms a diagonal matrix with elements of ρ_{b_m} along the diagonal. Additionally, the $N_{\mathrm{S}} \times N_T$ matrix of $\bar{\mathbf{H}} \triangleq \mathbf{W}_{\mathrm{D}}^{\mathrm{H}}\mathbf{A}_{\alpha}\mathbf{W}_{\mathrm{A}}^{\mathrm{H}}\mathbf{H}$ describes an equivalent channel matrix. Furthermore, the total additive noise vector $\bar{\mathbf{n}} \triangleq \mathbf{W}_{\mathrm{D}}^{\mathrm{H}}\mathbf{A}_{\alpha}\mathbf{W}_{\mathrm{A}}^{\mathrm{H}}\mathbf{n} + \mathbf{W}_{\mathrm{D}}^{\mathrm{H}}\mathbf{e} \in \mathbb{C}^{N_{\mathrm{S}} \times 1}$ in (5c) consists of the additive white Gaussian noise (AWGN) and a quantization noise term with the associated covariance matrix $\mathbf{R}_{\bar{\mathbf{n}}} \in \mathbb{C}^{N_{\mathrm{S}} \times N_{\mathrm{S}}}$ given by

$$\mathbf{R}_{\bar{\mathbf{n}}} = \mathbf{W}_{\mathrm{D}}^{\mathrm{H}}\mathbf{A}_{\alpha}\mathbf{W}_{\mathrm{A}}^{\mathrm{H}}\mathbf{R}_{\mathrm{n}}\mathbf{W}_{\mathrm{A}}\mathbf{A}_{\alpha}\mathbf{W}_{\mathrm{D}} + \mathbf{W}_{\mathrm{D}}^{\mathrm{H}}\mathbf{R}_{\mathrm{e}}\mathbf{W}_{\mathrm{D}}. \tag{6}$$

C. ACHIEVABLE SUM RATE AND ENERGY EFFICIENCY

Due to uncertainty on the Gaussian distribution of $\bar{\mathbf{n}}$, this phenomenon complicates the task of the ASR maximization. With these issues, some assumptions on the total additive noise vector are established to simplify our analysis in order to attain the lower bound ASR. Assume that $\hat{\mathbf{y}}$ is the new receiver signal vector, which is represented as

$$\hat{\mathbf{y}} = \bar{\mathbf{H}}\mathbf{x} + \hat{\mathbf{n}}, \tag{7}$$

where $\hat{\mathbf{n}}$ denotes a new total additive noise vector, which is a Gaussian distributed noise vector with the same covariance matrix as $\mathbf{R}_{\bar{\mathbf{n}}}$. In [23], it is shown that, for a given noise covariance matrix, the Gaussian distributed noise minimizes the mutual information. The objective is to design jointly the hybrid analog/digital combiners at the receiver end to optimize the lower bound of the ASR R_{lb}, given by

$$R_{\mathrm{lb}} = \log_2\left[\det(\mathbf{I}_{N_{\mathrm{S}}} + \frac{\mathbf{W}_{\mathrm{D}}^{\mathrm{H}}\mathbf{A}_{\alpha}\mathbf{W}_{\mathrm{A}}^{\mathrm{H}}\mathbf{H}\mathbf{R}_{\mathrm{xx}}\mathbf{H}^{\mathrm{H}}\mathbf{W}_{\mathrm{A}}\mathbf{A}_{\alpha}\mathbf{W}_{\mathrm{D}}}{\mathbf{R}_{\bar{\mathbf{n}}}})\right]. \tag{8}$$

TABLE I

THE VALUES OF ρ_m FOR DIFFERENT QUANTIZATION BITS b

b	1	2	3	4	5	>5
ρ_m	0.3634	0.1188	0.03744	0.01154	0.003490	$\frac{\pi\sqrt{3}}{2}2^{-2b}$

TABLE II

POWER CONSUMPTION OF HARDWARE COMPONENTS

Hardware Components	Symbol	Power Consumption
Baseband processor [4]	P_{D}	200 mW
ADC [14] [24]	P_{ADC}	Eq. (9)
RF chain [25]	P_{RF}	40 mW
Phase-shifter [26]	P_{PS}	40 mW
Switch [4]	P_{SW}	5mW
Inverter [4]	P_{IN}	5mW
Low noise amplifier [26]	P_{LNA}	20 mW

TABLE III

POWER CONSUMPTION OF EACH ARCHITECTURE

Architecture	Power Consumption
PS with the FC	$N_{\mathrm{R}}P_{\mathrm{LNA}} + N_{\mathrm{RF}}^{\mathrm{R}}P_{\mathrm{RF}} + N_{\mathrm{R}}N_{\mathrm{RF}}^{\mathrm{R}}P_{\mathrm{PS}} + 2P_{\mathrm{ADCtotal}} + P_{\mathrm{D}}$
PS with the GS-based FC	$N_{\mathrm{R}}P_{\mathrm{LNA}} + N_{\mathrm{RF}}^{\mathrm{R}}P_{\mathrm{RF}} + L_{\mathrm{R}}N_{\mathrm{RF}}^{\mathrm{R}}P_{\mathrm{PS}} + 2P_{\mathrm{ADCtotal}} + P_{\mathrm{D}}$
PS with the GS-based PC	$N_{\mathrm{R}}P_{\mathrm{LNA}} + N_{\mathrm{RF}}^{\mathrm{R}}P_{\mathrm{RF}} + L_{\mathrm{R}}P_{\mathrm{PS}} + 2P_{\mathrm{ADCtotal}} + P_{\mathrm{D}}$
SI with the FC	$N_{\mathrm{R}}P_{\mathrm{LNA}} + N_{\mathrm{RF}}^{\mathrm{R}}P_{\mathrm{RF}} + N_{\mathrm{R}}N_{\mathrm{RF}}^{\mathrm{R}}P_{\mathrm{SW}} + N_{\mathrm{RF}}^{\mathrm{R}}P_{\mathrm{IN}} + 2P_{\mathrm{ADCtotal}} + P_{\mathrm{D}}$
SI with the GS-based FC	$N_{\mathrm{R}}P_{\mathrm{LNA}} + N_{\mathrm{RF}}^{\mathrm{R}}P_{\mathrm{RF}} + L_{\mathrm{R}}N_{\mathrm{RF}}^{\mathrm{R}}P_{\mathrm{SW}} + N_{\mathrm{RF}}^{\mathrm{R}}P_{\mathrm{IN}} + 2P_{\mathrm{ADCtotal}} + P_{\mathrm{D}}$
SI with the GS-based PC	$N_{\mathrm{R}}P_{\mathrm{LNA}} + N_{\mathrm{RF}}^{\mathrm{R}}P_{\mathrm{RF}} + L_{\mathrm{R}}P_{\mathrm{SW}} + N_{\mathrm{RF}}^{\mathrm{R}}P_{\mathrm{IN}} + 2P_{\mathrm{ADCtotal}} + P_{\mathrm{D}}$

The power consumption of hardware components for each mmWave subarray architecture is summarized in Tables II and III. It should be pointed out that the activated antennas are reduced from N_{R} to L_{R} with the aid of the GS-based AS mechanism. The total power consumption of ADCs P_{ADCtotal} in Table III can be expressed as [11]-[12]

$$P_{\mathrm{ADCtotal}} = \sum_{m=1}^{N_{\mathrm{RF}}^{\mathrm{R}}} P_{\mathrm{ADC}}(b_m), \tag{9}$$

where $P_{\mathrm{ADC}}(b_m)$ represents the power consumption of the m-th ADC, which is defined as [12]

$$P_{\mathrm{ADC}}(b_m) = FOM_{\mathrm{W}} \cdot F_s \cdot 2^{b_m}, \tag{10}$$

where F_S is the Nyquist sampling rate, FOM_{W} is the Walden's figure-of-merit for evaluating the ADC's power efficiency, and b_m is the number of bits of the m-th RF chain. Notice that the shift power consumption of adaptively-switched mechanism on ADCs' precisions [14] is assumed to be zero in Tables II and III to further simplify the problem. Energy efficiency is defined as the ratio between the spectral efficiency and total power consumption P_{R}, which is given by

$$\eta_{\mathrm{EE}}(b_1,\ldots,b_{N_{\mathrm{RF}}^{\mathrm{R}}}) = \frac{R_{\mathrm{lb}}(b_1,\ldots,b_{N_{\mathrm{RF}}^{\mathrm{R}}})}{P_{\mathrm{R}}(b_1,\ldots,b_{N_{\mathrm{RF}}^{\mathrm{R}}})}. \tag{11}$$

III. GRAM-SCHMIDT BASED COMBINER DESIGN

In this section, to mitigate the hardware cost, an antenna selection mechanism is adopted to design the RF combiner for both the PS and SI based networks. The appropriate antenna set is concerned with the correlations between the selected antennas. The selecting procedure is accomplished by the GSO processes, which computes the projection height of each antenna and chooses the antennas corresponding to the largest L_{R} projection heights. The initialized antenna set before the GSO is denoted as $S_{b_0} = \{\ \}$. The receiver antenna set is described as $S_{Rx} = \{1, 2, \ldots, N_{\mathrm{R}}\}$, wherein the antenna indices are represented by the elements in this set. Additionally, the selected antenna indices are denoted by S_{b_k}, where the subscript b_k indicates the k-th orthogonal basis $\mathbf{b}_k$ and the k-th GSO step with $k = 1, 2, \ldots, L_{\mathrm{R}}$. The detailed manipulation in the GSO can be described as follows:

1) The first orthogonal basis $\mathbf{b}_1$ is determined by the largest norm among all row vectors of the channel matrix $\mathbf{H} = [\mathbf{h}_1, \ldots, \mathbf{h}_{N_{\mathrm{R}}}]^{\mathrm{T}}$. Here, $\mathbf{h}_n$ is defined as the n-th row vector of the matrix $\mathbf{H}$. Once the $\mathbf{b}_1$ is elected, the associated antenna index n_1 is settled. The processes of computing $\mathbf{b}_1$ and updating the associated index set are expressed as

$$\begin{aligned} \{\mathbf{b}_1, n_1\} &= \arg \max_{n \in S_{Rx}} (\|\mathbf{h}_n\|) \\ S_{b_1} &= S_{b_0} + \{n_1\} \end{aligned} \tag{12}$$

2) In the k-th GSO procedure, by means of projecting the remaining $(N_{\mathrm{R}} - k + 1)$ unselected channel row vectors onto the vector space spanned by the $(k-1)$ orthogonal bases denoted as $\mathrm{span}(\mathbf{b}_1, \ldots, \mathbf{b}_{k-1})$, the k-th orthogonal basis $\mathbf{b}_k$ is identified by the largest projection height. In the sequel, the corresponding antenna index set of S_{b_k} is updated accordingly. The above operation process can be described as

$$\{\mathbf{b}_k, n_k\} = \arg \max_{n \in S_{Rx} - S_{bk}} \left(\left\| \mathbf{h}_n - \sum_{j=1}^{|S_{bk}|} \frac{\langle \mathbf{h}_n, \mathbf{b}_j \rangle}{\|\mathbf{b}_j\|^2} \mathbf{b}_j \right\| \right), \quad (13)$$

$$S_{b_k} = S_{b_{k-1}} + \{n_k\},$$

where $|S_{b_k}|$ defines the cardinality of the subset S_{b_k}.

3) After the L_R antennas are selected, the selected antenna set $S_{b_{L_R}}$ have L_R indices, which is $\{n_1, \ldots, n_{L_R}\}$. Moreover, each RF chain must connect at least one antenna. On the other hand, the antenna i indices $\{n_1, \ldots, n_{N_{RF}^R}\}$ should be connected to the specified RF chain according to the subscript *k*. However, if L_R / N_{RF}^R exists remainder then the unconnected antenna indices $\{n_{1+N_{RF}^R}, \ldots, n_r\}$ have to be allocated to the corresponding RF chain, wherein *r* is the remainder.

It is evident that the complexity burden of the GSO process arises from the equations (12) and (13). By computing the norms of the row vectors of the channel matrix **H** in (12), the computational complexity requires $2N_R(N_T - 1)$ real additions and $4N_R N_T$ real multiplications. The overall computational complexity after executing sub-channel projections in (13) costs the total of $(2L_R - 1)(N_T - 1)N_T + 2(N_R - 1)N_T$ real additions and $4L_R(N_T - 1)N_T + 4(N_R + L_R)N_T$ real multiplications.

IV. ADC RESOLUTION MAPPING DESIGN

In this section, the ADC allocation design is based on the MSQE, which is defined by $\Phi(b) = \mathrm{E}[(Q(y_i) - y_i)^2]$, and the optimization problem is formulated as

$$(\hat{b}_1, \ldots, \hat{b}_{N_{RF}^R}) = \arg \min_{b_1, \ldots, b_{N_{RF}^R} \in K} \sum_{i=1}^{N_{RF}^R} \rho_b \mathrm{E}\left[|y_i|^2\right], \quad (14)$$

where $K \in \{1, 2, ..., 10\}$ denotes the ADC resolution set.

A. MINIMUM MEAN SQUARE QUANTIZATION ERROR BIT ALLOCATION

This algorithm was proposed by [14], adopting the total ADC power of the fixed resolution in each RF chain to be the constraint function of the optimization problem . The power limit of each RF chain is $P_{ADC}(\bar{b})$ which means all RF chain are deployed with the same ADC of $\bar{b}$ bits. $\bar{b}$ can also be regarded as the average value of total ADC in per RF chain. The optimization problem is rewritten as

$$(\hat{b}_1, \ldots, \hat{b}_{N_{RF}^R}) = \arg \min_{b_1, \ldots, b_{N_{RF}^R} \in K} \sum_{i=1}^{N_{RF}^R} \rho_b \mathrm{E}\left[|y_i|^2\right] \quad (15)$$

$$\text{s.t.} \sum_{i=1}^{N_{RF}^R} P_{ADC}(b_i) \le N_{RF}^R P_{ADC}(\bar{b}),\ \bar{b} \in K$$

where $\mathrm{E}[|y_i|^2] = \|[\mathbf{W}_A^H \mathbf{H}\mathbf{x}]_{i,:}\|^2 + 1$. By relaxing the condition $\hat{\mathbf{b}} = [\hat{b}_1, \cdots, \hat{b}_{N_{RF}^R}] \succ \mathbf{0}_{N_{RF}^R}$ to $\hat{\mathbf{b}} \succeq \mathbf{0}_{N_{RF}^R}$, the optimization problem can be solved by the Karush-Kuhn-Tucker (KKT) conditions in a closed form. The solution is derived as

$$\hat{b}_i = \bar{b} + \log_2 \left(\frac{N_{RF}^R \left(1 + \left\| \left[\mathbf{W}_A^H \mathbf{H}\mathbf{x}\right]_{i,:} \right\|^2\right)^{\frac{1}{3}}}{\sum_{j=1}^{N_{RF}^R} \left(1 + \left\| \left[\mathbf{W}_A^H \mathbf{H}\mathbf{x}\right]_{j,:} \right\|^2\right)^{\frac{1}{3}}} \right),\ i = 1, \ldots, N_{RF}^R, \quad (16)$$

where $\hat{b}_i$ is a real number. If $\hat{b}_i < 0$, the algorithm map $\hat{b}_i$ to zero and the others with non-zero or non-negative items are mapped to $\lceil \hat{b}_i \rceil$. In order to meet the limitation of total power in constraint function of the optimization problem, MMSQE-BA utilize a trade-off function to calculate the tradeoff value corresponding to the ADCs and sorting by the size. Finally, the tradeoff value in ascending sequence subtracts 1bit ADC until the total power meets the constraint of the constraint function. The trade-off function [14] is described as

$$F(i) = \frac{2^{-2\lfloor \hat{b}_i \rfloor} - 2^{-2\hat{b}_i}}{2^{\hat{b}_i} - 2^{\lfloor \hat{b}_i \rfloor}} \quad (17)$$

More detail description of the equation (17) is addressed in [14].

B. SUM-RESOLUTION ADC

Motivated by the constraint function in (15), this paper proposed a new ADC allocation algorithm based on the distinct constraint in the optimization problem. The total ADCs from all RF chains are adopted to be the constraint function. The solution from the SR-ADC algorithm must accord with the limitation of the constraint function which the total ADC must not exceed the preset upper bound denoted as b_{sum}. Note that $b_{average} = b_{sum} / N_{RF}^R$ denotes the average constraint resolution per RF chain and the optimization problem in (15) can be rewritten as

$$(\tilde{b}_1, \ldots, \tilde{b}_{N_{RF}^R}) = \arg \min_{b_1, \ldots, b_{N_{RF}^R} \in K} \sum_{i=1}^{N_{RF}^R} \rho_b \mathrm{E}\left[|y_i|^2\right]$$
$$\text{s.t.} \sum_{i=1}^{N_{RF}^R} b_i \le b_{sum},\ b_{sum} \in \{1, 2, 3, \ldots, 40\} \quad (18)$$

Similar to the MMSQE-BA, by relaxing the condition $\tilde{\mathbf{b}} = [\tilde{b}_1, \ldots, \tilde{b}_{N_{RF}^R}] > \mathbf{0}_{N_{RF}^R}$ to $\hat{\mathbf{b}} \succeq \mathbf{0}_{N_{RF}^R}$ the optimization problem can be solved by the KKT conditions and obtain a solution in a closed form, which is derived as

$$\tilde{b}_i = \frac{b_{sum}}{N_{RF}^R} + \frac{1}{2N_{RF}^R} \sum_{j=1}^{N_{RF}^R} \log_2 \left(\frac{1 + \left\| \left[\mathbf{W}_A^H \mathbf{H}\mathbf{x}\right]_{i,:} \right\|^2}{1 + \left\| \left[\mathbf{W}_A^H \mathbf{H}\mathbf{x}\right]_{j,:} \right\|^2} \right),\ i = 1, \ldots, N_{RF}^R, \quad (19)$$

where $\tilde{b}_i$ is a real number. In order to meet the results of

This article has been accepted for publication in a future issue of this journal, but has not been fully edited. Content may change prior to final publication. Citation information: DOI 10.1109/ACCESS.2021.3070116, IEEE Access

TABLE IV

Sum-Resolution ADC algorithm

Input : b_{sum}, $N_{\text{RF}}^{\text{R}}, S=\{1,2,\ldots,N_{\text{RF}}^{\text{R}}\}$
for $i=1\cdots N_{\text{RF}}^{\text{R}}$
Compute $(\hat{b}_1,\ldots,\hat{b}_{N_{\text{RF}}^{\text{R}}})$ using (19)
$\hat{b}_i=\max\left(0,\left\lceil\hat{b}_i\right\rceil\right)$
end
$b_{\text{total}}=\text{sum}\left(\hat{b}\right)$
while $b_{\text{total}}>b_{\text{sum}}$
$g'=\arg\max_{i\in S}\hat{b}_i$
$\hat{b}_{g'}=\hat{b}_{g'}-1$ and $S=S-\{g'\}$
if $\left(\hat{b}_{g'}<0\right), \hat{b}_{g'}=0$
if $\left(\text{isempty}(S)==1\right), g_2'=0, S=1:N_{\text{RF}}^{\text{R}}, g_2'=\arg\max_{i\in S}\hat{b}_i$ and $g'=g_2'$
end
return b

(19) we map the negative terms into zero and map the non-zero terms into non-negative integer $\lceil\tilde{b}_i\rceil$. With the total ADC constraint in (18), the limitation of the upper bound of total ADC is satisfied by the following steps:

Step 1) Arrange the order of $\tilde{\mathbf{b}}$ in a decreasing sequence and subtract 1 bit ADC according to the sequence. The revised ADC ceases the adjustment step and moves to next unrevised ADC.

Step 2) If total ADC is incompatible with the limitation of constraint after step1, repeat step1 until the total bit meets the constraint function in (18). For the purpose of improving energy efficiency, this paper employs the MMSQE-BA and SR-ADC algorithms in PS-based and SI-based network with varieties of antenna allocation architectures. Both the dynamic CSC and GS based RF-antenna mappers are employed to achieve an extra saving on the quantity of PSs compared with the fully-connected architecture. Additionally, the SI-based hybrid precoding subarray employs the GS AS technique to decrease the amounts of receiver antennas and switches. Remarkably, the situation of a 0-bit ADC may occur whether the MMSQE-BA or SR-ADC algorithm is adopted. The power can be saved by turning off the process of RF chain with the 0-bit ADC and the output becomes zero.

The dominant computational complexity of the SR-ADC approach is incurred by the computation of $\mathbf{W}_{\text{A}}^{\text{H}}\mathbf{Hx}$ of the equation (19), which is given as $2N_{\text{RF}}^{\text{R}}(N_{\text{R}}-1)+2N_{\text{R}}(N_{\text{T}}-1)$ real additions and $4N_{\text{RF}}^{\text{R}}N_{\text{R}}+4N_{\text{R}}N_{\text{T}}$ real multiplications. Therefore, the total computational complexity ends up with $2N_{\text{RF}}^{\text{R}}(2N_{\text{RF}}^{\text{R}}+N_{\text{R}})+2N_{\text{R}}(N_{\text{T}}-1)+2(b_{\text{total}}-b_{\text{sum}})$ real additions and $4N_{\text{RF}}^{\text{R}}(3N_{\text{RF}}^{\text{R}}+N_{\text{R}}+3)+4N_{\text{R}}N_{\text{T}}$ real multiplcations by the algorithm in Table IV. The operation philosophy of the SR-ADC technique is similar to that of the MMSQE-BA and thus accomplish an approximate computational complexity. With the utilization of the GS AS strategy, the computational complexity of the SR-ADC is slightly higher than that of the MMSQE-BA. When solving the optimization problem by means of the Matlab CVX toolbox, it is difficult to evaluate the pratical computational complexity of the CVX-based technique. The complexity of the CVX-based scheme can be estimated by observing the program operation-time, which is much higher than the SR-ADC scheme.

V. SIMULATION RESULTS

In this section, the simulations evaluate energy efficiency as a function of SNR for a mmWave massive MIMO uplink hybrid combing system with the ADC allocation algorithm proposed in the paper. The architecture of RF network adopt PS-based and SI-based. USPA configuration are employed on the base station with $N_{\text{S}}=4$, $N_{\text{T}}=64$, $N_{\text{R}}=64$, and $N_{\text{RF}}^{\text{T}}=N_{\text{RF}}^{\text{R}}=32$ over the SV channel with $P=10$ and $I=8$. The angles of departure (AODs) and arrival (AOAs) are distributed uniformly in $[-\pi,\pi]$ and $[-\pi/2,\pi/2]$, respectively. The azimuth angle-spread of each angle is assumed to be 5 degrees. The simulation results are obtained from the average results of 1000 iterations. In the following figures, "PS" and "SI" denote the phase shifter network and switch-inverter network, respectively. "FC" represents the fully-connected architecture. "GS56" denotes the hybrid combiner based on the Gram-Schmidt antenna selection mechanism and the number of the selected antennas is $L_{\text{R}}=56$. "MMSQE_b", "SR-ADC_b", and "CVX_b" are the ADC allocation schemes with the average constraint bit $b_{average}$.

Fig. 3 illustrates the achievable sum-rate with different ADC resolution configuration of the average constraint bit $b_{average}=2,4,6,8,10$ as a function of SNR for fully-connected hybrid combing architecture. The results show that the employment of low average constraint bit leads to the serious performance degradation in high SNR regime. The degradation problem can be effectively improved by adopting higher average constraint bit and can achieve the maximum sum-rate at $b_{average}=10$. It also can be seen that all the ADC bit allocation schemes proposed in this paper provide a better sum rate performance.

Fig. 4 plots the comparison of the energy efficiency with several ADC resolution configurations for the same architecture in Fig. 3 To clearly point out the influence of different average constraint bit for the system performance, we utilize $b_{average}=2,4,6,8,10$ and plot the energy efficiency as a function of SNR. It shows that all the proposed ADC bit allocation schemes provide the better EE performance with $b_{average}=2,4,6$ and increase monotonically with different $b_{average}$ at low SNR regime. However, the performance degradation emerges from lower average constraint bit $b_{average}=2,4$ at high SNR regime. Moreover, the results demonstrate that $b_{average}=6$ provides the better

This article has been accepted for publication in a future issue of this journal, but has not been fully edited. Content may change prior to final publication. Citation information: DOI 10.1109/ACCESS.2021.3070116, IEEE Access

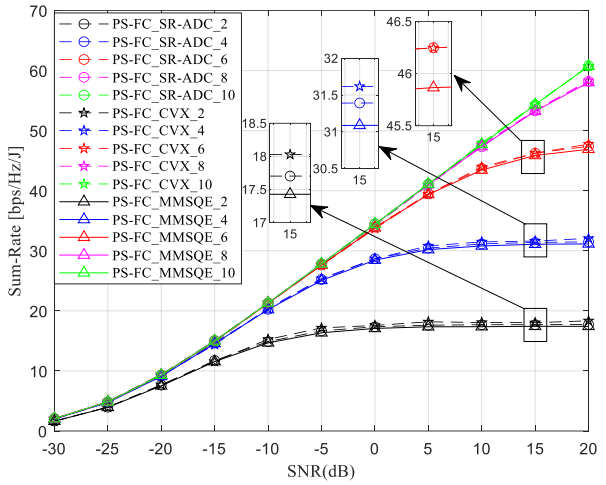

FIGURE 3. **Achievable sum rate with $b_{average}$=2,4,6,8,10 bits of the fully connected architecture as a function of SNR.**

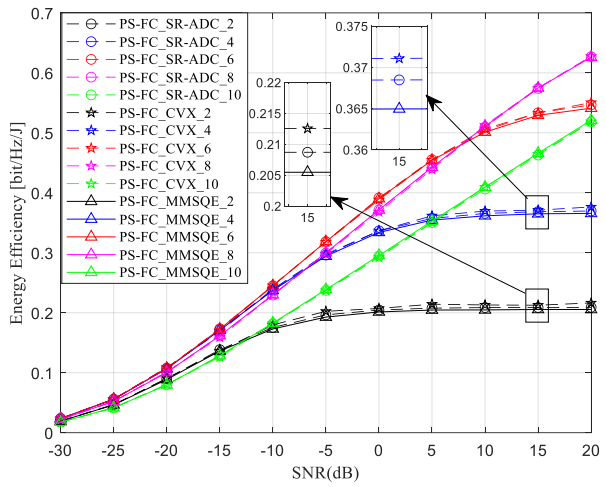

FIGURE 4. **Energy efficiency with $b_{average}$=2,4,6,8,10 bits of the fully connected architecture as a function of SNR.**

performance before SNR=10dB and $b_{average} = 8$ possesses the maximum EE after SNR=10dB.

Fig. 5 illustrates the influence of different antenna selection number L_R on sum rate as a function of average constraint bit $b_{average}$ for SR-ADC bit allocation scheme at SNR=15dB. The results show that sum rate increases as the number of L_R and achieves the maximum performance after $b_{average} = 8$. Furthermore, it can be seen from the figure that the sum rate gap remains constant in the low average constraint bit at first and becomes denser in the high constraint bit region.

Results of Fig. 6 present the influence of different antenna selection number L_R on energy efficiency as a function of average constraint bit $b_{average}$ for the SR-ADC bit allocation scheme at SNR=15dB . It can be seen that the performance of EE increases as the reduced antenna selection shifters, causing the lower power consumption.

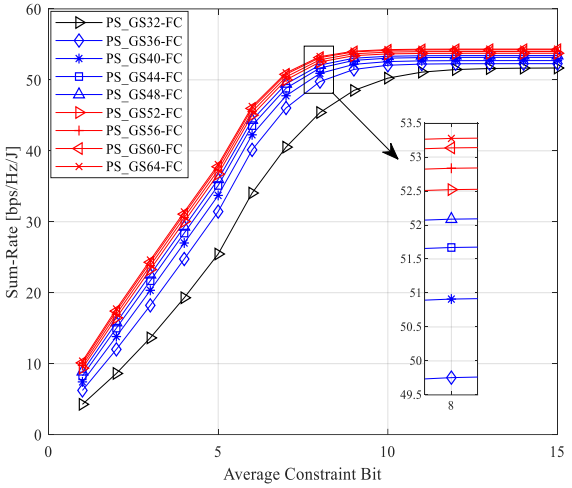

FIGURE 5. **Achievable sum rate of SR-ADC versus different L_R as a function of average constraint bit at SNR=15dB.**

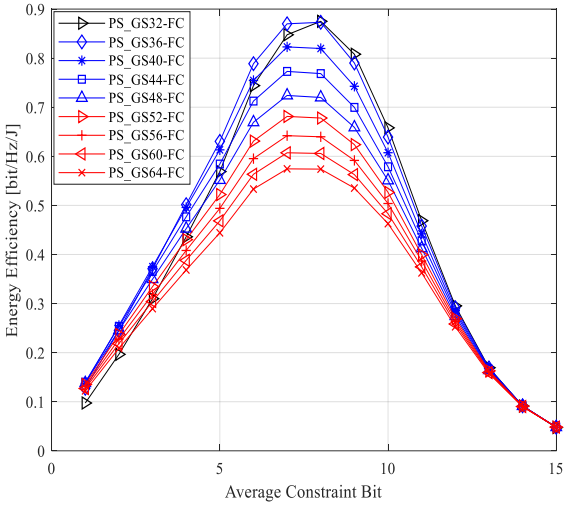

FIGURE 6. **Energy efficiency of SR-ADC versus different L_R as a function of average constraint bit at SNR=15dB.**

While the GS36 requires $4N_{RF}^{R}$ (128) more phase shifters than the GS32, the GS36 provides better EE performance owing to the huge performance gap of ASR between the GS32 and GS36 before $b_{average} = 8$. Consequently, it is demonstrated that both ASR and EE are influenced by the antenna selection number L_R considerably, and $b_{average} = 8$ can achieve the near-optimal performance considering the trade-off between the system throughput and power consumption for antenna selection mechanism. In addition, L_R must be at least a mean value of N_{RF}^{R} and N_R to remain the ASR performance. In this paper, L_R is set to the mean value of $L_R = 48$ and $N_R = 64$ ($L_R = 56$) as the representative of antenna selection mechanism.

In Fig. 7, the results present the ASR performance with different ADC allocation schemes as a function of average constraint bit $b_{average}$ for various hybrid combining architectures at high SNR region (SNR=15B). The results

This article has been accepted for publication in a future issue of this journal, but has not been fully edited. Content may change prior to final publication. Citation information: DOI 10.1109/ACCESS.2021.3070116, IEEE Access

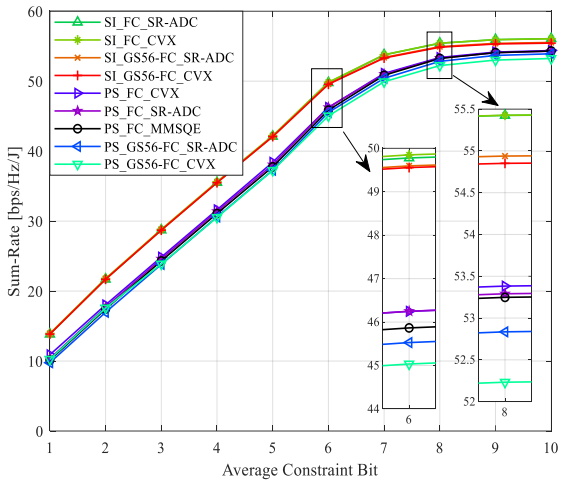

FIGURE 7. Achievable sum rate with various of ADC allocation schemes as a function of average constraint bit for different architecture at SNR=15dB.

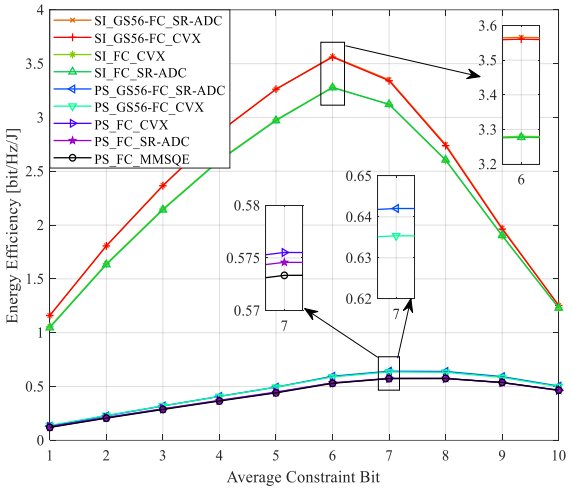

FIGURE 8. Energy efficiency with various of ADC allocation schemes as a function of average constraint bit for different architecture at SNR=15dB.

show that all the ADC allocation schemes in SI-based provide superior ASR performance than PS-based and the ASR capacity-gap between the different networks reduce as the increase of average constraint bit. It is observed that the CVX based and SR-ADC offer the better ASR than MSQE-BA in PS-based. Furthermore, both the CVX based and SR-ADC achieve the near-optimal ASR for different hybrid combining architectures after $b_{average} = 8$.

The results of Fig. 8 present the EE performance with different ADC allocation schemes as a function of average constraint bit for various hybrid combining architectures at high SNR region (SNR=15dB). It is observed that CVX based and SR-ADC provide excellent EE performance in SI-based compared to PS-based. However, the performance gap between the CVX based and SR-ADC is very small. The simple closed form solution of SR-ADC provides the advantage with low computation complexity compared to CVX based. The reason is that the CVX toolbox would be time consuming when processes the convex optimization

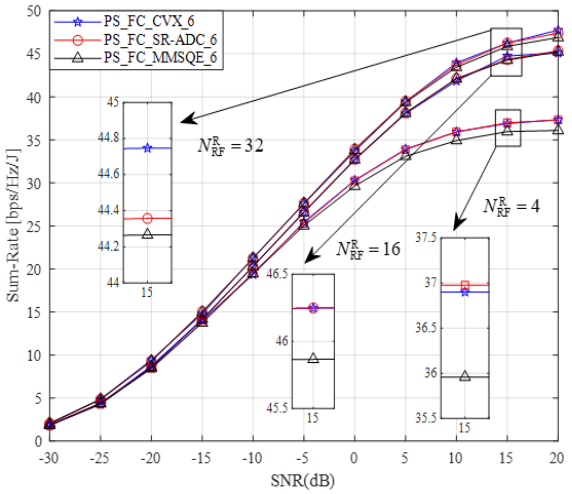

FIGURE 9. Achievable sum rate with $b_{average}$=6 bits on the fully connected architecture as a function of SNR for different RF chain number.

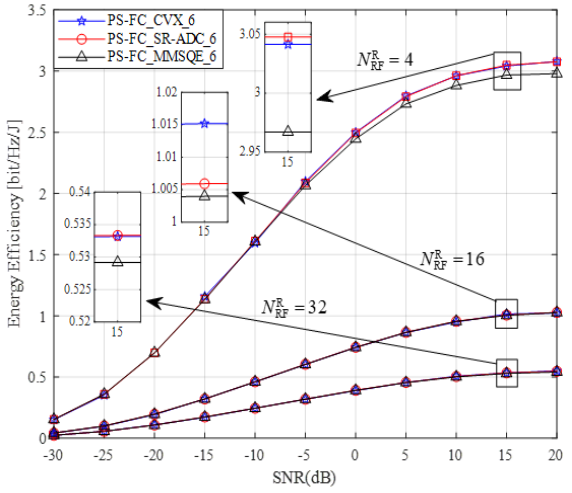

FIGURE 10. Energy efficiency with $b_{average}$=6 bits on the fully connected architecture as a function of SNR for different RF chain number.

problem with logarithmic and exponential function. Moreover, it can be seen that both the CVX based and SR-ADC offer the better EE performance compared to MMSQE-BA. The configuration of the average constraint bit with the optimal EE performance in PS-based and SI-based are $b_{average} = 7$ and $b_{average} = 6$, respectively.

Fig. 9 illustrates the influence of different RF chain number on ASR with various ADC allocation schemes as a function of SNR for fully-connected architecture $b_{average} = 6$. The results show that all the proposed ADC allocation schemes provide better ASR performance than MMSQE-BA with $N_{RF}^{R} = 4, 16, 32$ and the performance gap becomes larger as the reduction of RF chain number.

Fig. 10 plots the influence of different RF chain number on EE with various ADC allocation schemes as a function of SNR for fully-connected architecture at $b_{average} = 6$. As the number of RF chain increases, it can be seen from the results that the performance gap between the proposed

This article has been accepted for publication in a future issue of this journal, but has not been fully edited. Content may change prior to final publication. Citation information: DOI 10.1109/ACCESS.2021.3070116, IEEE Access

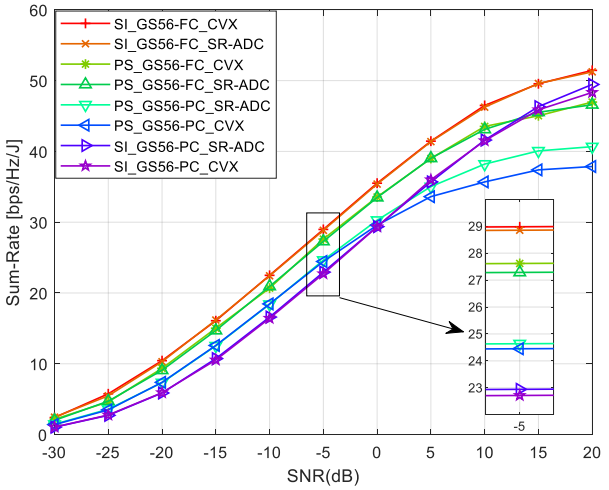

FIGURE 11. Achievable sum rate with the GS antenna selection mechanism as a function of SNR for the fully- and partially-connected architecture at $b_{average}$=6 bits.

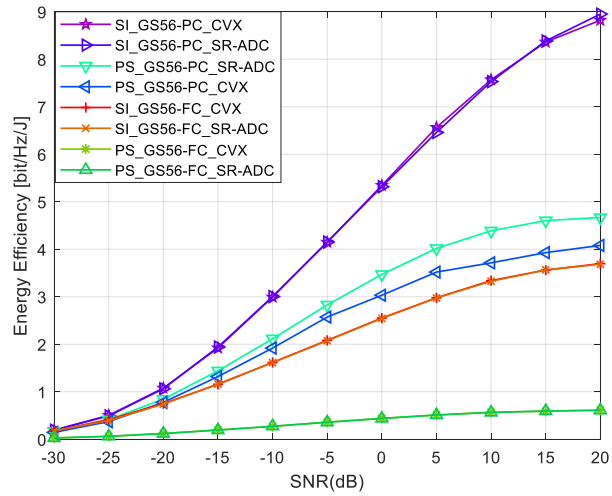

FIGURE 12. Energy efficiency with the GS antenna selection mechanism as a function of SNR for the fully- and partially-connected architecture at $b_{average}$=6 bits.

ADC allocation schemes and MMSQE-BA becomes small due to the more power consumption from RF chains and ADCs. Consequently, it is demonstrated that the proposed schemes can achieve superior performance both on the ASR and EE with different numbers of RF chains.

Figs. 11 and 12 present the ASR and EE performance with the use of the proposed ADC allocation schemes as a function of SNR for the FC and PC based hybrid combining architectures at 6 average constraint bits. Results show that all the EE performance of the PC structure outperforms the SI_GS56-PC after SNR=0 dB. Furthermore, it can be seen that the SR-ADC provides better performance on the ASR and EE than that of the CVX method at the PS_GS56-PC architecture, while the performance gap between, the SR-ADC and the CVX algorithms is unobvious for other hybrid combining schemes. Consequently, the SR-ADC approach has an obvious advantage compared to the CVX based method.

VI. CONCLUSION

In order to improve the overall energy efficiency in the massive MIMO system, the SR-ADC algorithm based on MSQE is proposed and utilizes the number of total bits from all RF chain to be the constraint of the optimization problem. To achieve the optimal trade-off between ASR and EE, this paper employs the fixed antenna subarray and the GS-based antenna selection mechanism for both PS-based and SI-based network. Remarkably, the combination architecture of dynamically-mapped ADC bit resolution and dynamically-connected subarray pattern is capable of providing superior hardware benefits. Additionally, the adaptive subarray arrangement in conjunction with the GS-based AS strategy able to accomplish the EE performance much better than those of approaches without the GS AS with an alleviated demand on both computation and hardware complexities. Moreover, simulation results demonstrate that the proposed algorithm outperforms the MMSQE-BA algorithm in low average ADC range for both networks. Finally, we investigate the number of total ADCs with best EE performance in all antenna allocation configurations and demonstrate the performance in terms of SNR.

APPENDIX

According to [18], $\rho_b \mathrm{E}[|y_i|^2]$ can be approximated to $\frac{\pi\sqrt{3}}{2} v_i 2^{-2b_i}$, where $v_i = [\mathbf{W}_{\mathrm{A}}^{\mathrm{H}} \mathbf{H} \mathbf{x}]_{i,:}$. In order to obtain the equivalent convex optimization problem from (18), we can obtain the results of $b_i = \frac{-1}{2}\log_2 d_i$ and $b_{\mathrm{sum}} = \frac{-1}{2}\log_2 d_{\mathrm{sum}}$ by defining $d_i = 2^{-2b_i}$ and $d_{\mathrm{sum}} = 2^{-2b_{\mathrm{sum}}}$. Thus, the equation (18) is re-expressed as

$$(\hat{b}_1, \ldots, \hat{b}_{N_{\mathrm{RF}}^{\mathrm{R}}}) = \arg \min_{b_1,\ldots,b_{N_{\mathrm{RF}}^{\mathrm{R}}} \in K} \sum_{i=1}^{N_{\mathrm{RF}}^{\mathrm{R}}} v_i d_i \tag{20a}$$

$$\text{s.t. } \log_2 d_{\mathrm{sum}} - \sum_{i=1}^{N_{\mathrm{RF}}^{\mathrm{R}}} \log_2 d_i \le 0 \,,\ \mathbf{D} \succ \mathbf{0}_{N_{\mathrm{RF}}^{\mathrm{R}}} , \tag{20b}$$

where $\hat{\mathbf{b}} = [\hat{b}_1, \ldots, \hat{b}_{N_{\mathrm{RF}}^{\mathrm{R}}}]^{\mathrm{T}}$ and $\mathbf{0}_{N_{\mathrm{RF}}^{\mathrm{R}}}$ denotes as the $N_{\mathrm{RF}}^{\mathrm{R}} \times 1$ zero vector. The objective function in (15) can be reformulated as $\sum_{i=1}^{N_{\mathrm{RF}}^{\mathrm{R}}} v_i d_i = \mathbf{V}^{\mathrm{T}}\mathbf{D}$. In addition, the problem in (20) is equivalent to (18) and is a convex optimization problem. Consequently, the global optimal solution can be obtained by the KKT condition. At first, we relax $\mathbf{D} \succ \mathbf{0}_{N_{\mathrm{RF}}^{\mathrm{R}}}$ to $\mathbf{D} \succeq \mathbf{0}_{N_{\mathrm{RF}}^{\mathrm{R}}}$ for the purpose of obtaining the Lagrange dual function, which is described as

$$L(\mathbf{D}, \lambda, \upsilon) = \mathbf{V}^{\mathrm{T}}\mathbf{D} + \lambda \left(\log_2 d_{\mathrm{sum}} - \sum_{i=1}^{N_{\mathrm{RF}}^{\mathrm{R}}} \log_2 d_i \right) + \boldsymbol{\upsilon}^{\mathrm{T}} (-\mathbf{D}), \tag{21}$$

where λ and $\boldsymbol{\upsilon} = [\upsilon_1, \cdots, \upsilon_{N_{\mathrm{RF}}^{\mathrm{R}}}]^{\mathrm{T}}$ are the Lagrange multiplier associated with the constraint functions in (20). From (21), the gradient of the Lagrangian with respect to $\mathbf{D}$ is acquired

as

$$\nabla_{\mathbf{D}} L(\mathbf{D},\lambda,\upsilon)=\frac{\partial \mathbf{V}^{\mathrm{T}}\mathbf{D}}{\partial \mathbf{D}}+\frac{\partial}{\partial \mathbf{D}}\left(\left[\lambda,\upsilon_1,\ldots,\upsilon_{N_{\mathrm{RF}}^{\mathrm{R}}}\right]\begin{bmatrix}\log_2 d_{\mathrm{sum}}-\sum_{i=1}^{N_{\mathrm{RF}}^{\mathrm{R}}}\log_2 d_i\\ -\mathbf{D}\end{bmatrix}\right)$$
$$=\mathbf{V}+\left[\mathbf{G},-\mathbf{I}_{N_{\mathrm{RF}}^{\mathrm{R}}}\right]\begin{bmatrix}\lambda\\ \boldsymbol{\upsilon}\end{bmatrix}=\mathbf{0}_{N_{\mathrm{RF}}^{\mathrm{R}}}, \quad (22)$$

where $\mathbf{G}=[-d_1^{-1},\cdots,-d_n^{-1}]^{\mathrm{T}}$ is the Jacobian matrix of $\mathbf{D}$ with $n=N_{\mathrm{RF}}^{\mathrm{R}}$. From (20a), (20b), and (22), the KKT condition can be written as

$$\log_2 d_{\mathrm{sum}}-\sum_{i=1}^{N_{\mathrm{RF}}^{\mathrm{R}}}\log_2 d_i\le 0,\ -\mathbf{D}\preceq \mathbf{0}_{N_{\mathrm{RF}}^{\mathrm{R}}} \quad (23a)$$

$$\lambda\ge 0,\ \boldsymbol{\upsilon}\succeq \mathbf{0}_{N_{\mathrm{RF}}^{\mathrm{R}}} \quad (23b)$$

$$\lambda\left(\log_2 d_{\mathrm{sum}}-\sum_{i=1}^{N_{\mathrm{RF}}^{\mathrm{R}}}\log_2 d_i\right)=0,\ \boldsymbol{\upsilon}^{\mathrm{T}}(-\mathbf{D})=0 \quad (23c)$$

$$\nabla_{\mathbf{D}} L(\mathbf{D},\lambda,\upsilon)=\mathbf{V}+\left[\mathbf{G},-\mathbf{I}_{N_{\mathrm{RF}}^{\mathrm{R}}}\right]\begin{bmatrix}\lambda\\ \boldsymbol{\upsilon}\end{bmatrix}=\mathbf{0}_{N_{\mathrm{RF}}^{\mathrm{R}}}, \quad (23d)$$

where (23a)-(23d) denote as the primal constraint, the dual constraint feasibility, and the complementary slackness in the KKT conditions. From (23c), the inference for $\boldsymbol{\upsilon}=\mathbf{0}_{N_{\mathrm{RF}}^{\mathrm{R}}}$ is guaranteed owing to $\mathbf{D}\succ\mathbf{0}_{N_{\mathrm{RF}}^{\mathrm{R}}}$. By applying the above results in (23d), it can be demonstrated that $\mathbf{V}=-\lambda\mathbf{G}$ and the result of $\lambda\neq 0$ is met, while satisfying $\mathbf{V}\neq\mathbf{0}_{N_{\mathrm{RF}}^{\mathrm{R}}}$ and $\mathbf{G}\neq\mathbf{0}_{N_{\mathrm{RF}}^{\mathrm{R}}}$. As a consequence, the relation is described as

$$v_i=\lambda/d_i \quad (24a)$$

$$\sum_{i=1}^{N_{\mathrm{RF}}^{\mathrm{R}}}\log_2 d_i=\log_2 d_{\mathrm{sum}} \quad (24b)$$

After some manipulations of (24a) and (24b), the global optimal solution can be established as follows:

$$\hat{b}_i=\frac{b_{\mathrm{sum}}}{N_{\mathrm{RF}}^{\mathrm{R}}}+\frac{1}{2N_{\mathrm{RF}}^{\mathrm{R}}}\sum_{j=1}^{N_{\mathrm{RF}}^{\mathrm{R}}}\log_2\left(\frac{1+\|v_i\|^2}{1+\|v_j\|^2}\right),\ i=1,\ldots,N_{\mathrm{RF}}^{\mathrm{R}} \quad (25)$$

From (25), it can be seen that the closed form solution of $\hat{b}_i$ complies with the KKT conditions since $\hat{b}_i>0$. Finally, the equation of (19) can be achieved by utilizing $v_i=[\mathbf{W}_{\mathrm{A}}^{\mathrm{H}}\mathbf{H}\mathbf{x}]_{i,:}$ into (25).

REFERENCES

[1] J. G. Andrews *et. al.*, "What will 5G be?" *IEEE J. Sel. Areas Commun.*, vol. 32, no. 6, pp. 1065–1082, Jun. 2014.

[2] F. Sohrabi and W. Yu, "Hybrid digital and analog beamforming design for large-scale antenna arrays," *IEEE J. Sel. Topics Signal Process.*, vol. 10, no. 3, pp. 501–513, Apr. 2016.

[3] R. Méndez-Rial, C. Rusu, N. González-Prelcic, A. Alkhateeb, and R. W. Heath, Jr., "Hybrid MIMO architectures for millimeter wave communications: Phase shifters or switches?" *IEEE Access*, vol. 4, pp. 247–267, Jun. 2016.

[4] X. Gao, L. Dai, Y. Sun, S. Han, and C.-L. I, "Machine learning inspired energy-efficient hybrid precoding for mmWave massive MIMO systems," in *2017 IEEE Int. Conf. Commun.* (ICC), Paris, France, May 2017, pp. 1–6.

[5] L. N. Ribeiro, S. Schwarz, M. Rupp, and Andr´e L. F. de Almeida, "Energy efficiency of mmWave massive MIMO precoding with low-resolution DACs," *IEEE J. Sel. Top. Signal Process.*, vol. 12, no. 2, pp. 298–312, May 2018.

[6] Q. Ding, Y. Deng, and X. Gao, "Spectral and energy efficiency of hybrid Precoding for mmWave massive MIMO with low-resolution ADCs/DACs," *IEEE Access*, vol. 7, pp. 186529–186537, 2019.

[7] S. Ghacham, M. Benjillali, L. Van der Perre, and Z. Guennoun, "Rate analysis of uplink massive MIMO with low-resolution ADCs and ZF detectors over Rician fading channels," *IEEE Commun. Lett.*, vol. 23, no. 9, pp. 1631–1635, Sep. 2019.

[8] A. Mezghani, R. Ghiat, and J. A. Nossek, "Transmit processing with low resolution D/A-converters," in *Proc. of 16th IEEE Int. Conf. Electron., Circuits, Syst.*, Yasmine Hammamet, Tunisia, Dec. 2009, pp. 683–686.

[9] A. Mezghani and J. A. Nossek, "Capacity lower bound of MIMO channels with output quantization and correlated noise," in *Proc. IEEE Int. Symp. on Inform. Theory* (ISIT), Cambridge, MA, USA, Jul. 2012, pp. 1–5.

[10] N. Liang and W. Zhang, "Mixed-ADC massive MIMO," *IEEE J. Sel. Areas Commun.*, vol. 34, no. 4, pp. 983–997, Apr. 2016.

[11] J. Zhang, L. Dai, Z. He, S. Jin, and X. Li, "Performance analysis of mixed-ADC massive MIMO systems over Rician fading channels," *IEEE J. Sel. Areas Commun.*, vol. 35, no. 6, pp. 1327–1338, Jun. 2017.

[12] Y. Zhang, M. Zhou, H. Cao, L. Yang, and H. Zhu, "On the performance of cell-free massive MIMO with mixed-ADC under Rician fading channels," *IEEE Commun. Lett.*, vol. 24, no. 1, pp. 43–47, Jan. 2020.

[13] C.-C. Hu, W.-C. Lin, and W.-S. Liao, "Hybrid precoding mmWave massive MIMO systems with dynamic resolution DAC," in *Proc. of IEEE 7th Global Conf. Consumer Electron.* (GCCE), Nara, Japan, Oct. 2018, pp. 134–135.

[14] J. Choi, B. L. Evans, and A. Gatherer, "Resolution-adaptive hybrid MIMO architectures for millimeter wave communications," *IEEE Trans. Signal Process.*, vol. 65, no. 23, pp. 6201–6216, Dec. 2017.

[15] K.-G. Nguyen, Q.-D. Vu, L.-N. Tran, and M. Juntti, "Energy-efficient bit allocation for resolution-adaptive ADC in multiuser large-scale MIMO systems: Global optimality, " in *Proc. of IEEE Int. Conf. Acoustics, Speech and Signal Process.* (ICASSP), Barcelona, Spain, May 2020, pp. 5130-5134.

[16] J.-C. Chen, "Spectral- and energy-efficient hybrid receivers for millimeter-wave massive multiuser MIMO uplink systems with variable-resolution ADCs," *IEEE Syst. J.*, pp. 1–9, May 2020. (early access)

[17] H. Sheng, X. Chen, X. Zhai, A. Liu, and M.-J. Zhao, "Energy efficiency optimization for millimeter wave system with resolution-adaptive ADCs," *IEEE Wireless Commun. Lett.*, vol. 9, no. 9, pp. 1519-1523, Sep. 2020.

[18] C.-C. Hu and C.-W. Hsu, "Efficient adaptive subarrays in millimeter-wave MIMO systems with hybrid RF/baseband precoding/combining design," *IEEE Syst. J.*, vol. 13, no. 4, pp. 3735–3746, Dec. 2019.

[19] C.-C. Hu and J.-H. Zhang, "Hybrid precoding design for adaptive sub-connected structures in millimeter-wave MIMO systems," *IEEE Syst. J.*, vol. 13, no. 1, pp. 137–146, Mar. 2018

[20] C.-C. Hu and H.-Y. Yang, "Modified Gram-Schmidt-based antenna selection for MIMO systems in correlated channels," *Electron. Lett.*, vol. 46, no. 1, pp. 94–96, Mar. 2010.

[21] J. Max, "Quantizing for minimum distortion," *IRE Trans. Inform. Theory*, vol. 6, no. 1, pp. 7–12, Mar. 1960.

[22] A. K. Fletcher, S. Rangan, V. K. Goyal, and K. Ramchandran, "Robust predictive quantization: Analysis and design via convex optimization," *IEEE J. Sel. Topics Signal Process.*, vol. 1, no. 4,

pp. 618–632, Dec. 2007.

[23] S. N. Diggavi and T. M. Cover, "Worst additive noise under covariance constraints," *IEEE Trans. Inform. Theory*, vol. 47, no. 7, pp. 3072–3081, Nov. 2001.

[24] S. Cui, A. J. Goldsmith, and A. Bahai, "Energy-constrained modulation optimization," *IEEE Trans. Wireless Commun*., vol. 4, no. 5, pp. 2349–2360, Sep. 2005.

[25] R. W. Heath, Jr., N. Gonzalez-Prelcic, S. Rangan, W. Roh, and A. M. Sayeed, "An overview of signal processing techniques for millimeter wave MIMO systems," *IEEE J. Sel. Top. Signal Process*., vol. 10, no. 3, pp. 436–453, Apr. 2016.

[26] E. Bjornson, L. Sanguinetti, J. Hoydis, and M. Debbah, "Optimal design of energy-efficient multi-user MIMO systems: Is massive MIMO the answer?" *IEEE Trans. Wireless Commun.*, vol. 14, no. 6, pp. 3059–3075, Jun. 2015.

Chia-Chang Hu received the B.S. and M.S. degrees from the National Cheng Kung University, Tainan, Taiwan, in 1990 and 1992, respectively, and the Ph.D. degree from the University of Southern California, Los Angeles, CA, in 2002, all in electrical engineering. Since February 2003, he has been with the Department of Communications Engineering, National Chung Cheng University, Chia-Yi, Taiwan, where he is currently a Full Professor. His current research interests are in the areas of communication theory and advanced signal processing for communications, with a special emphasis on statistical signal and array processing, wireless multiuser communications, wideband CDMA, ultra-wideband technology, relay/antenna selection strategy and precoding design for wireless relay-assisted networks, and millimeter-wave communication techniques.

Yong-Siang Li was born in Taiwan, 1993. He received the B.S. and M.S. degrees from the Yuan Ze University, Taoyuan, Taiwan, and the National Chung Cheng University, Chia-Yi, Taiwan, in 2015 and 2020, respectively, all in communications engineering. His research interests include the ADC resolution algorithm design and the hybrid precoding design in millimeter-wave communication systems.

Chen-Yueh Lin was born in Taiwan, 1995. He received the B.S. degree in communications engineering from the National Central University, Taoyuan, Taiwan, in 2019. He is currently working toward the M.S. degree in communications engineering at the National Chung Cheng University, Chia-Yi, Taiwan. His research interests include the DAC resolution algorithm design and the hybrid precoding design for the generalized spatial modulation aided millimeter-wave communication systems.